https://ntrs.nasa.gov/search.jsp?R=19930084225 2020-06-17T17:09:17+00:00Z

NACA TN 3419

NATIONAL ADVISORY COMMITTEE FOR AERONAUTICS

TECHNICAL NOTE 3419

NACA MODEL INVESTIGATIONS OF SEAPLANES IN WAVES

By John B. Parkinson

Langley Aeronautical Laboratory
Langley Field, Va.

Washington
July 1955

1X

NATIONAL ADVISORY COMMITTEE FOR AERONAUTICS

TECHNICAL NOTE 3419

NACA MODEL INVESTIGATIONS OF SEAPLANES IN WAVES[1]

By John B. Parkinson

SUMMARY

The characteristics of seaplanes in rough water are investigated experimentally in the Langley tanks by means of self-propelled dynamically similar models having freedom in the vertical plane. Time histories are obtained of required quantities during simulated take-offs and landings into transverse waves of various sizes.

The maximum trim, rise, vertical acceleration, and angular acceleration during a number of landings are used as criteria for comparisons. For landings in waves of a given height, the criteria are primarily dependent on wave length and usually peak at a critical wave length. Significant reductions in the motions and accelerations are obtained by practical increases in hull length-beam ratio, afterbody length, angle of dead rise, and suitable combinations of these features. The normal impact load is a function of hull trim, flight-path angle, and vertical velocity at contact, referred to the local wave slope and wave velocity. The measured maximum vertical accelerations and the associated effective contact parameters from tests in various heights of waves are largely functions of the wave height-length ratio. Vertical loads calculated from the experimental contact parameters are in reasonable agreement with the vertical accelerometer data. The mean resistance to motion through waves is higher than the resistance in smooth water. The increment is greatest at intermediate speeds during take-off where rebounds are most severe.

INTRODUCTION

Waves are of importance in aeronautics because even relatively mild sea conditions induce critical loads and uncontrollable motions on seaplanes. These adverse effects have imposed severe additional design requirements on an already compromised class of aircraft and have generally limited open-sea operations to acceptance trials or emergencies such as sea rescue. In recent years, jet-assisted take-off and reversible propellers for landing have improved the situation somewhat by shortening the

---

[1]Paper presented at Conference on Ships and Waves, Stevens Institute of Technology, Oct. 25-27, 1954.

high-speed portions of the runs in waves; nevertheless the problem of the all-weather water-based aircraft has not yet been satisfactorily solved, and there has been an increasing necessity for more effective solutions.

The National Advisory Committee for Aeronautics conducts continuing research programs on the fundamental aspects of water impact loads due to waves and the rough-water behavior of seaplane configurations. The purposes of this activity are to develop improved methods for predicting water loads and pressures and better means of alleviating the adverse effects induced by wave encounter.

Experimental phases of the work are carried out in the large-scale hydrodynamic facilities of the NACA located at the Langley Aeronautical Laboratory at Langley Field, Va. The Langley impact basin (ref. 1) is a highly specialized facility for establishing basic relationships among the impact parameters. The Langley tanks are generally similar in function and operation to towing basins designed to test ship models except that they have relatively higher carriage speeds to accommodate the large Froude numbers associated with water-based aircraft.

SYMBOLS

b	beam of hull, ft
g	acceleration due to gravity
H	wave height, ft
L	distance from forward perpendicular to sternpost, ft
$\frac{R + D}{wb^3}$	total-resistance coefficient
V	speed, fps
V_h	horizontal velocity, fps
V_r	resultant velocity, fps
V_{r_e}	effective resultant velocity, fps
V_v	vertical velocity, fps
V_{v_e}	effective full-scale vertical velocity, fps

V_w wave velocity, fps

γ flight-path angle, deg

γ_e effective flight-path angle, deg

θ angle of inclination of water surface, deg

λ wave length, ft

τ trim of straight portion of forebody, deg

τ_e effective trim, deg

DESCRIPTION OF TANKS

Langley Tank No. 1

Langley tank no. 1 was placed in operation in 1931 (ref. 2) and enlarged in 1937 (ref. 3). It has a width of 24 feet, a maximum depth of 12 feet, and a maximum speed of 60 miles per hour. With the installation of a wave maker and beaches at the ends, the working length is approximately 2,800 feet. This installation is shown in figure 1.

The working element of the wave maker is a transverse flat plate, hinged at the bottom and oscillated by a link at the top connected to an adjustable-radius crank. The crank is driven through a gear reducer by a 75-horsepower direct-current electric motor. The rotational speed of the motor is controlled by varying its input voltage from a constant-speed motor-generator set. The length and height of the waves are varied by adjusting the speed of the motor and the radius of the crank.

Tests of complete seaplane models in calm water are made at the 6-foot level in this tank to improve the air flow over the aerodynamic surfaces, and wave suppressors have been installed at this level to reduce the time between runs. For tests in waves, the water is raised to the 8.5-foot level (see fig. 1) to deactivate the wave suppressors and provide greater displacement for the plate. Waves propagated northward are dissipated on the slotted concrete beach shown. Those waves propagated southward travel through the test region against the motion of the models and are dissipated on a similar beach located at the south end of the tank.

The polygonal cross section of Langley tank no. 1 eventually introduces undesirable variations in the wave characteristics across the tank. These effects are minimized by calibration, testing as close to the wave

maker as possible, and using only the first waves produced before interference patterns build up. With such precautions and continuous monitoring of the waves in the test region, satisfactory duplication of test conditions and results are obtained.

The ranges of wave size available at the 8.5-foot level are shown in figure 2. The heights are limited by a theoretical upper boundary, derived by equating the maximum triangular area swept by the plate to the area of trochoidal waves of various sizes above the still-water level. Actual regular waves are obtained close to this boundary. At short wave lengths, the heights become irregular as indicated by the left-hand shaded boundary. Regular wave heights below 1 foot for tests of seaplane models cannot be produced with length-height ratios of much less than 25 or 30.

Langley Tank No. 2

Langley tank no. 2 was completed in 1942 and is located alongside the first. It has a working length of approximately 1,730 feet, a width of 18 feet, a uniform depth of 6 feet, and a maximum towing speed of 60 miles per hour. From experience with the first tank, the towing carriage of Langley tank no. 2 was made much smaller to minimize aerodynamic interference on complete seaplane models. This feature was made possible by the use of closely spaced rails supported by the roof-truss system.

Langley tank no. 2 is rectangular in cross section with continuous concrete beaches along both sides at the water line to suppress waves between runs. For tests in waves, the water level is dropped below the beaches. Since the water depth is then constant over the width, transverse waves remain uniform for a longer period than in the first tank, and regular waves with length-height ratios as low as 12 to 15 are available. The wave maker and end beaches are similar in principle to those provided for Langley tank no. 1, and the apparatus and procedures for tests in waves in the two tanks are also similar.

DYNAMIC MODELS

A 1/10-size powered dynamic model of a twin-engine flying boat set up for tests in waves in Langley tank no. 1 is shown in figure 3. It is geometrically similar in essential respects to the full-scale seaplane and is ballasted to have scale gross weight, scale position of center of gravity, and scale longitudinal radius of gyration. The propellers are of scale diameter and are driven by variable-frequency alternating-current electric motors to produce scale thrust. The wing flaps are

adjustable and the elevators are adjustable or controllable to suit the conditions to be simulated.

The particulars of the model are necessarily related to those of the full-scale airplane by Froude's law of comparison to obtain geometrically similar wave and spray patterns and proper scaling of the hydrodynamic forces. If viscous effects are neglected, this law applies equally to the aerodynamic forces; the wing, however, must be fitted with leading-edge slats, which are not on the full-scale seaplane, to prevent a large loss of lift at high angles of attack due to the low model Reynolds number.

The Froude number is also the criterion for dynamic similarity of any geometrically similar systems moving under the predominant influence of inertia and gravity forces. When the Froude relationships for speed, size, mass, and mass distribution are satisfied, the relative positions of the systems after proportional periods of time are the same and motion paths of corresponding points in space are geometrically similar. This general principle is used to advantage in aeronautical research for model investigations of highly complex flight problems, such as the prediction of flying qualities, spin recovery, and motions in gusts, as well as the behavior of seaplanes on the water.

With ballasting for scale ellipsoid of inertia and with the addition of the side stabilizing floats of the full-scale seaplane, the tank model can be operated completely free of the towing carriage for observations of its three-dimensional behavior and can even be operated outdoors for a closer simulation of wind and sea conditions in nature.

APPARATUS AND PROCEDURE

Towing Gear

For the determination of critical behavior in the vertical plane during take-off and landing runs, it is advantageous to use the towing carriage to restrain the model laterally and in roll and yaw, as well as to carry along observers and equipment. A side view of the model, together with the towing gear developed for this purpose, is shown in figure 4.

The model is attached to a light vertical staff, which has a pivot at the model center of gravity permitting freedom in trim and which passes through a roller cage that allows vertical motion only and provides the lateral restraint. The roller cage is free to move fore and aft along the track shown; thus this motion allows the model to check properly in waves. Stops with pneumatic shock absorbers limit the longitudinal and

vertical motion with respect to the carriage, and data are preferably taken only when the model is free of the stops. Connections to the model are attached near the pivot to minimize their restraint on the trim motions. The arrangement is shown schematically in figure 5.

The model is fixed in trim during a landing approach with fixed elevators by a solenoid-operated brake that releases automatically when one of the keel contacts first touches the water. This procedure eliminates rotation due to ground effect and simulates more closely a full-scale piloted glide.

After contact, the elevators of the model normally remain fixed. They are also on occasion controlled from the carriage by the model "pilot" or automatically by angular displacement and rate senstive mechanisms to simulate the rapid corrective actions instinctively taken by experienced pilots.

Instrumentation

Vertical acceleration is measured by an accelerometer on the staff attached to the model and angular acceleration, by a matched pair of accelerometers in the model near the center of gravity. (See fig. 5.) These units are commercial oil-damped, variable-resistance types having fundamental frequencies of the order of 100 to 200 cycles per second. The small variations in voltage they produce are utilized to modulate a stronger carrier signal produced by a 5-kilocycle electronic oscillator. The modulated carrier is amplified and then rectified in a bridge-demodulator circuit to provide a suitable input to the oscillograph. The recording units of the latter have lower natural frequencies of the order of 35 cycles per second to minimize extraneous "hash" due to high-frequency vibration.

Trim, rise, and fore-and-aft motion with respect to the carriage are recorded by resistance slide-wire pickups at appropriate points, connected through direct-current bridge circuits to the oscillograph. Contact with the water at various points along the keel is registered by platinum loops in the nonconducting material of the model that complete circuits to ground when wetted.

Wave profiles with respect to the carriage are recorded by platinum strips mounted on sharp-edged struts located fore and aft and off to one side of the model. Current flowing through these circuits to ground varies with the height of the water on the struts. The resulting traces on the oscillograph show the general shape of the waves and location of the crests but do not provide accurate measurements of the wave heights; the measurements are better obtained from float recorders and visual observations at the monitoring station in the test region of the tank.

The instantaneous speed of the towing carriage is recorded by a direct-current generator geared to a guide wheel. The distance traveled by the carriage is registered by a light-beam photocell unit interrupted by shutters along the track. Oscillograph records from the photocell unit calibrate the speed records from the generator. The towing force applied by the towing spring is recorded by a high-frequency resistance strain gage in series with the towing line. Power for the electrical units is obtained from the carriage service trolleys and from storage batteries as indicated in figure 5.

Records and Interpretation

A typical oscillograph record of a model landing in oncoming waves is shown in figure 6. The time interval indicated is 1/10 of a second. On the left, the model is flying above the water against the rear stop with landing power, the elevators are set for the landing attitude, and the trim brake is locked. As the carriage is decelerated, the model moves forward off the rear stop and goes into a free steady glide as indicated by the straight portion of the rise trace. At the first contact with the water, indicated by the stop contact trace, the trim brake is released and the model goes into a series of rebounds off the waves during which the motions and accelerations become progressively more severe until speed is lost and the model follows the waves to rest.

Although the first contact is random, the subsequent traces for repeat runs in the same wave trains are remarkably similar, and four to eight runs are usually sufficient to establish consistent maximum values of trim, rise, and accelerations (ref. 4). This degree of reproducibility is attained because in regular wave trains the motions induced by the initial contact are small in comparison with the subsequent rebounds below flying speed, and the latter are largely the consequence of meeting the next wave upslope after contact, even though a downslope or trough may be contacted first.

In addition to the initial and maximum values of the motions and accelerations, the records yield corresponding values of the horizontal speed, vertical speed (slope of the rise curve), and trim at each contact for detailed analysis of the impacts. Motion pictures of the runs are also made to aid in interpretation of the data and to record the spray characteristics. The motion pictures projected at the Froude time scale provide an opportunity to judge the behavior and make comparisons on the basis of the corresponding full-size time scale.

Take-off tests are made with full thrust and with the carriage accelerated to keep the model clear of the stops until flying speed is reached. In general, similar behavior and comparable values of acceleration are experienced as for landings, although more rebounds are induced over a longer period of time.

TYPICAL RESULTS AND DISCUSSION

Effects of Hull Proportions

Figure 7 illustrates a related family of hulls for the same flying boat having wide variations in the basic design parameter of the length-beam ratio. The lowest ratio is representative of practice as recent as World War II. The highest ratio represents an extreme from practical considerations.

The size and aerodynamic drag of these hulls decrease as the length-beam ratio increases, whereas the smooth-water hydrodynamic qualities remain more or less comparable throughout the series (refs. 5, 6, and 7). Tank investigations in waves of the type described have demonstrated significant effects of the higher ratios with regard to rough-water qualities as shown in figure 8 (data from refs. 7 and 8). The maximum values of the criteria for behavior are plotted against wave length in feet (full scale) for a constant wave height of 4 feet (full-scale). The curves are faired upper envelopes of the data from a number of landings at each wave length tested. Maximum trim and rise are indicative of the extent of attitudes reached above the stall and heights reached above the water during rebounds. The accelerations are indicative of relative load factors on structures supporting concentrated masses in the airplane (ref. 9).

The plots illustrate the general dependence (ref. 4) of the adverse effects for a given wave height on wave length. Usually there is a critical wave length at which the effects are most severe. This critical length does not have a universal relationship to hull length and must be determined for each configuration and wave height.

As the length-beam ratio is increased, the maximum values of trim, rise, and vertical acceleration are progressively reduced. (See fig. 8.) These effects are interdependent since the milder impacts result in lower rebounds, and vice versa. The narrower beam hulls also benefit from the fundamental load-alleviating effects of more chine immersion and lower aspect ratio of the forebody wetted area involved in the impacts. The maximum angular acceleration increases somewhat because of the increase in length inherent in the series, although the acceleration for L/b of 20 and 15 are approximately the same. In spite of this increase, the resultant loads, particularly near the center of gravity, are significantly alleviated.

Effects of Hull Form

Figure 9 summarizes data similar to those presented in figure 8 for various modifications of the model with a length-beam ratio of 15, which

is chosen as the upper practical limit. The top curves in each case are for the basic hull of length-beam ratio 15. The short-dash—long-dash curves (from ref. 10) indicate a marked improvement obtained by extending the afterbody length to match the length required by the tail surfaces. The increase in bearing aft greatly reduces the trim and rise motions and the accelerations are significantly smaller, particularly near the critical wave length. Similar results were obtained in an earlier investigation (ref. 4) of a model with a low length-beam ratio.

A second logical improvement is a large increase in V-bottom dead-rise angle, in this case from a conventional 20° to 40° (ref. 11). Figure 9 shows that the motions and angular acceleration were not greatly changed. The large decrease in vertical acceleration, other things being equal, is predictable from theory. The important contribution of the dynamic-model investigation (ref. 11) is that the high-dead-rise form was apparently satisfactory in other respects and even higher dead-rise angles than 40° may be of some practical interest for still greater load alleviation.

The short-dash curves (from ref. 12) indicate that the two previous features can be combined for further gains. In this modification, the dead-rise angle of the long-afterbody hull was progressively increased from the step to the bow. The combination has lower motions than the basic hull of length-beam ratio 15 and the lowest accelerations of the series. When compared with the data in figure 8 for a length-beam ratio of 6, it has 9° less maximum trim, 8 feet less maximum rise, and the maximum vertical and angular accelerations are reduced in the order of 60 percent.

Effects of Wave Proportions

The results presented so far were all for one height of wave. Corresponding data have been obtained for the hulls with length-beam ratios of 6 and 15 of the series in various heights of waves corresponding to 2, 4, and 6 feet (full-scale). (See ref. 8.) The trends obtained are complex in that the maximum values for the two higher waves remain about the same but the critical wave lengths are displaced; this displacement indicates a primary dependence on the maximum wave slope.

The raximum normal impact load of a prismatic forebody is a theoretical function of the trim, flight-path angle, and vertical velocity at contact with the water surface, as well as the dead-rise angle and the load (ref. 13). The theory is applied to the rough-water case by redefining the contact angles relative to the wave slope and taking into account the velocity increments due to the wave motion (refs. 14 and 15). The relationships of the contact parameters measured in the tests and the effective parameters in waves given by Miller (ref. 14) are illustrated in figure 10.

The symbol θ is the local slope of the wave surface at contact, τ is the trim of the straight portion of the forebody, and γ is the flight-path angle or the angle of the resultant velocity V_r; all are referred to the horizontal. A simple and adequate assumption for the velocity increments of the wave, according to the theory of reference 14, is that the wave may be considered a body of water in horizontal translation at the wave velocity V_w. Adding V_w to the horizontal speed V_h gives the effective resultant velocity V_{r_e}.

From figure 10, the effective contact parameters determining the water load are

$$\tau_e = \tau - \theta$$

$$V_{v_e} = V_v \cos \theta + \left(V_h + V_w\right) \sin \theta$$

$$\gamma_e = \theta + \tan^{-1} \frac{V_v}{V_h + V_w}$$

Since the angles are small, the normal load is approximately equal to the vertical load measured on the model.

Figure 11 shows values of maximum vertical acceleration and the associated effective contact parameters for the model with a length-beam ratio of 6 landing in various heights and lengths of waves plotted against the wave height-length ratio. The points shown are for the maximum impacts only obtained in the three heights of wave, and they were computed directly from the tabular data (ref. 8). Since the wave speeds and slopes at contact were not actually measured, it was assumed that the maximum impacts occurred on the maximum slopes of the tank waves and that these waves were trochoidal. The slope for the calculations is then

$$\theta = \tan^{-1} \frac{\pi H}{\lambda}$$

and the wave speed is

$$V_W = \sqrt{\frac{g\lambda}{2\pi}}$$

where H and λ are the wave height and wave length, respectively.

Except for the effective trim, the plotted points for the three wave heights lie for the most part along smooth upper envelopes drawn from the origins; this indicates the adequacy of the assumptions and the primary dependence of the results on the wave slope. The effective trim points are more scattered but have a downward trend with increase in wave slope as represented by the mean line shown.

The severity of the impacts for the model configuration investigated appears to peak at an H/λ of around 0.025 or a length-height ratio of 40. At these ratios, the effective trim is as low as 4°, the effective full-scale vertical velocity is as high as 30 feet per second, and the effective flight-path angle is as much as 15°. Since the corresponding loads are very high from a structural point of view, it is of interest to compute the vertical accelerations by the method of reference 14 for a rigid prismatic planing surface from values of the contact parameters from the mean line and faired envelopes of the figure. The results are shown by the dashed line (see fig. 11(a)) and indicate reasonable agreement with the experimental data, considering the inherent limitations of both methods. The fact that the experimental accelerations are higher than the theoretical is significant since it indicates that the instrumentation chosen is not attenuating high-frequency loads of importance.

Figure 11(b) presents data for the model with a length-beam ratio of 15 (ref. 8). The data show trends similar to those presented in figure 11(a); hence, the trends are the same over a wide range of hull proportions. The effective trims are as low as 0° (flat impact) as compared with 4° in figure 11(a), the maximum effective full-scale vertical velocities are reduced from 30 to 25 feet per second, the maximum effective flight-path angle from 15° to 12°, and the highest maximum vertical accelerations from 12.5g to 9.5g. The agreement of the measured accelerations with those calculated from theory is closer than that for $L/b = 6$ because the additional alleviation due to chine immersion associated with the higher length-beam ratio is not taken into account in the method of calculation used (ref. 15).

This method of analysis suggests a useful purpose of the model tests in addition to that of obtaining comparative information. Engineering calculations of design impact-load factors require the effective contact parameters to be assumed. These assumptions are normally established by experience with conventional seaplanes for the initial impact only. When applied to unconventional configurations they

sometimes lead to dubious results by not taking into account all the influences on the motions prior to the critical impact. In such cases the range of contact parameters deduced from model tests provide a more realistic basis for design estimates of the maximum loads.

Take-Off Resistance in Waves

The resistance of seaplanes during take-off remains a problem of some importance in spite of the increases in thrust afforded by present developments in powerplants. The resistance becomes greater in rough water because of the added energy in the motions and the increased wetting of parts of the airplane that remain dry in smooth-water operation.

The magnitude of the increase in the case of a configuration similar to figure 3 is indicated by the data plotted in figure 12. The points are the total average resistance (R + D), measured by the strain-gage dynamometer described previously, at a succession of constant speeds throughout the take-off range. The center-of-gravity position and elevator deflection are constant. The ordinate and abscissa are in terms of Froude nondimensional coefficients proportional to total resistance and speed, respectively. The take-off thrust available, in terms of a corresponding coefficient, is shown on the plot for comparison.

The lower solid curve is for the smooth-water resistance and illustrates the critical points of minimum thrust available for acceleration at the hump speed and near take-off. In 2- and 4-foot waves, the resistance is progressively higher at intermediate planing speeds, where the motions and extra wetting due to waves and spray thrown are greatest. At the hump speed, where the model can more or less follow the wave contours, the resistance is about the same as in smooth water. Near take-off, where the model is nearly airborne, the motions and wetting again become small, and the resistance tends to again approach the smooth-water values. In 6-foot waves, the hump resistance becomes much higher because the model can no longer ride over the crests and the aerodynamic components are heavily wetted.

Figure 12 indicates that, with the available thrust shown, the design would not take off in waves higher than 2 feet. This conclusion of course does not take into account the favorable effects of wind normally present in practice and any favorable scale effects on the aerodynamic and hydrodynamic forces. It does, however, illustrate the need for jet-assisted take-off for open-sea operation in swells and defines a problem that can become more severe in the future for closely coupled jet-propelled configurations.

CONCLUDING REMARKS

The NACA seaplane tanks have been provided with wave makers, apparatus, and instrumentation for investigations of seagoing qualities of water-based aircraft. The operation of Froude dynamic models in the tank waves has served to aid in defining the problems and the relative importance of some of the many parameters. Several practicable design improvements offering significant alleviation of the adverse effects of waves have been developed. General relationships of the qualities of importance in rough-water take-offs and landings with wave length and length-height ratio have been demonstrated. The increase in take-off resistance due to rough water has been investigated briefly and apparently can be critical for operation in large waves.

Langley Aeronautical Laboratory,
National Advisory Committee for Aeronautics,
Langley Field, Va., May 25, 1955.

REFERENCES

1. Batterson, Sidney A.: The NACA Impact Basin and Water Landing Tests of a Float Model at Various Velocities and Weights. NACA Rep. 795, 1944. (Supersedes NACA WR L-163.)

2. Truscott, Starr: The N.A.C.A. Tank - A High-Speed Towing Basin for Testing Models of Seaplane Floats. NACA Rep. 470, 1933.

3. Truscott, Starr: The Enlarged N.A.C.A. Tank, and Some of Its Work. NACA TM 918, 1939.

4. Benson, James M., Havens, Robert F., and Woodward, David R.: Landing Characteristics in Waves of Three Dynamic Models of Flying Boats. NACA TN 2508, 1952. (Supersedes NACA RM L6L13.)

5. Yates, Campbell C., and Riebe, John M.: Effect of Length-Beam Ratio on the Aerodynamic Characteristics of Flying-Boat Hulls. NACA TN 1305, 1947.

6. Carter, Arthur W., and Haar, Marvin I.: Hydrodynamic Qualities of a Hypothetical Flying Boat With a Low-Drag Hull Having a Length-Beam Ratio of 15. NACA TN 1570, 1948.

7. Carter, Arthur W., and Whitaker, Walter E., Jr.: Effect of an Increase in Hull Length-Beam Ratio From 15 to 20 on the Hydrodynamic Characteristics of Flying Boats. NACA RM L9G05, 1949.

8. Carter, Arthur W.: Effect of Hull Length-Beam Ratio on the Hydrodynamic Characteristics of Flying Boats in Waves. NACA TN 1782, 1949.

9. Parkinson, John B.: Appreciation and Determination of the Hydrodynamic Qualities of Seaplanes. NACA TN 1290, 1947.

10. Kapryan, Walter J., and Clement, Eugene P.: Effect of Increase in Afterbody Length on the Hydrodynamic Qualities of a Flying-Boat Hull of High Length-Beam Ratio. NACA TN 1853, 1949.

11. Whitaker, Walter E., Jr., and Bryce, Paul W., Jr.: Effect of an Increase in Angle of Dead Rise on the Hydrodynamic Characteristics of a High-Length-Beam-Ratio Hull. NACA TN 2297, 1951.

12. Kapryan, Walter J.: Effect of Forebody Warp and Increase in Afterbody Length on the Hydrodynamic Qualities of a Flying-Boat Hull of High Length-Beam Ratio. NACA TN 1980, 1949.

13. Milwitzky, Benjamin: Generalized Theory for Seaplane Impact. NACA Rep. 1103, 1952.

14. Miller, Robert W.: Hydrodynamic Impact Loads in Rough Water for a Prismatic Float Having an Angle of Dead Rise of 30°. NACA TN 1776, 1948.

15. Schnitzer, Emanuel: Theory and Procedure for Determining Loads and Motions in Chine-Immersed Hydrodynamic Impacts of Prismatic Bodies. NACA Rep. 1152, 1953. (Supersedes NACA TN 2813.)

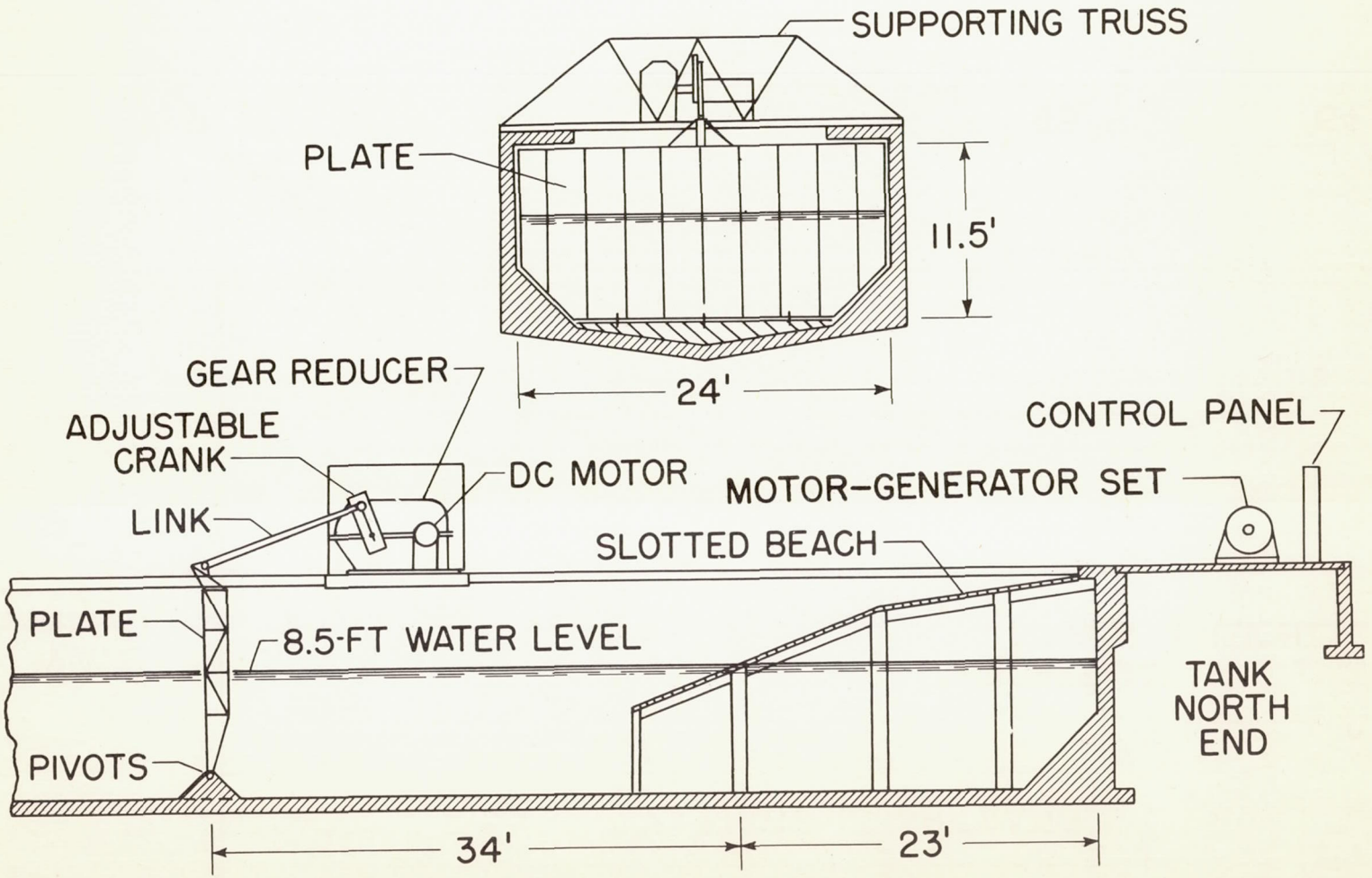

Figure 1.- Wave maker and beach in Langley tank no. 1.

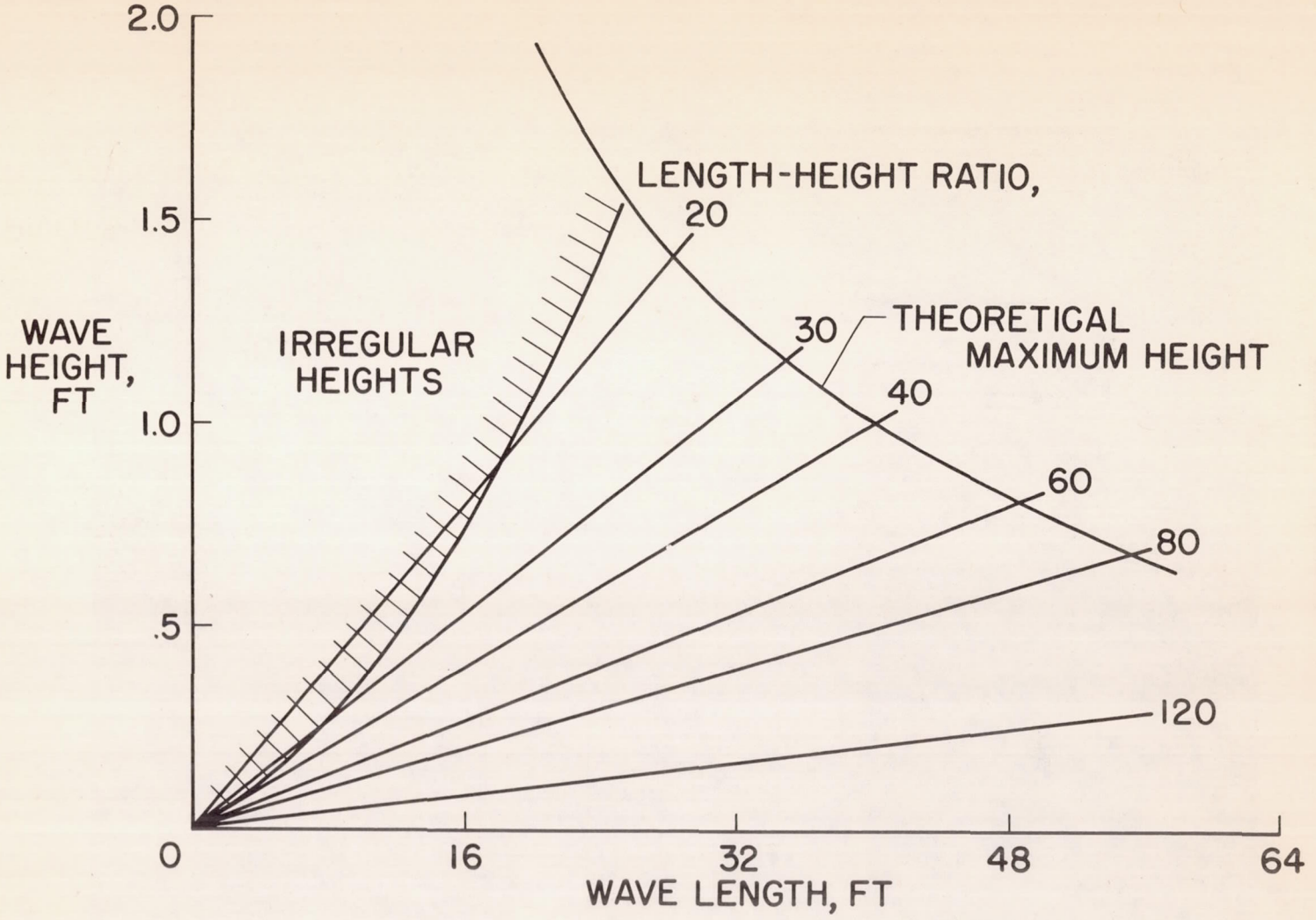

Figure 2.- Working range of Langley tank no. 1 wave maker at 8.5-foot water level.

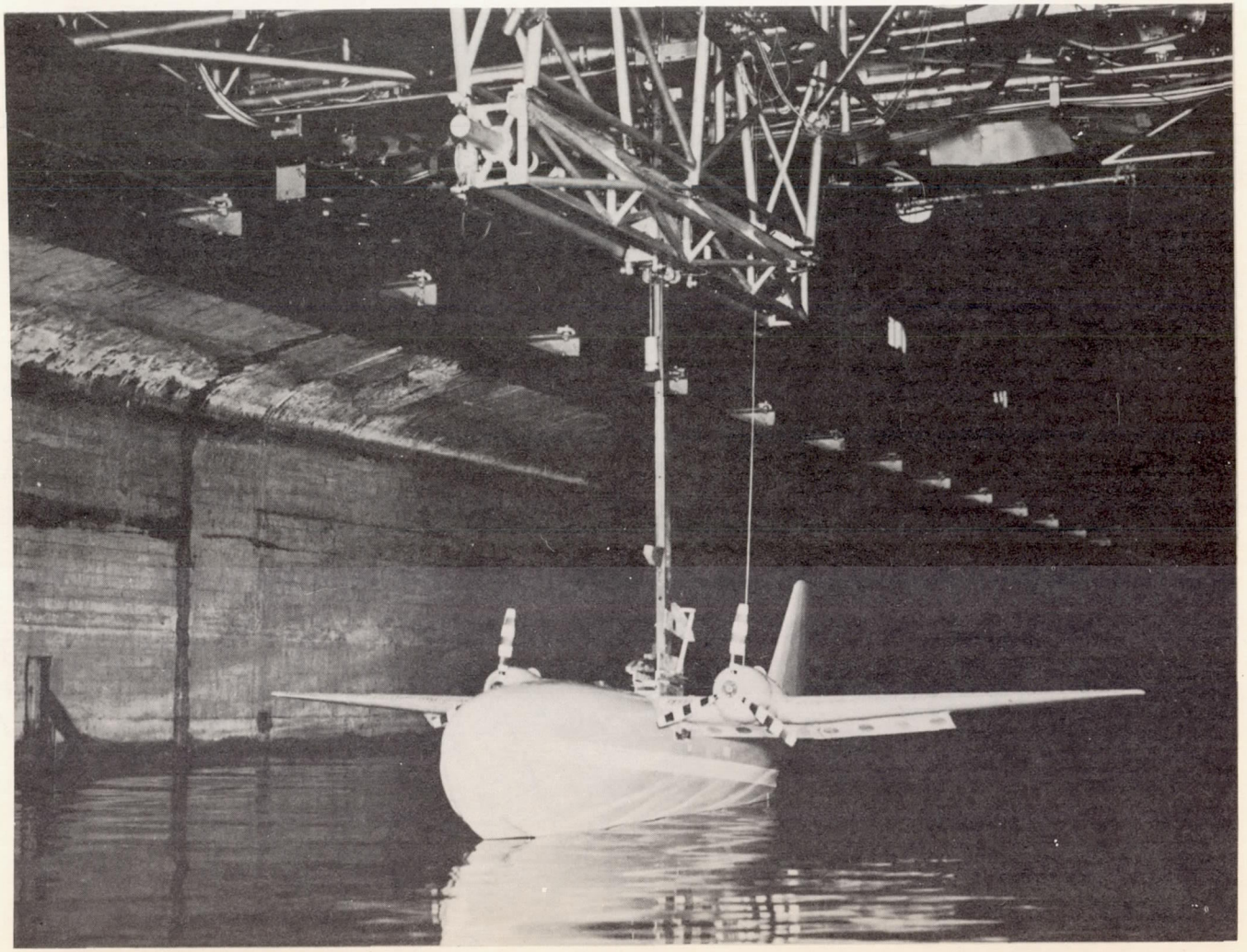

Figure 3.- Typical powered dynamic model for tests in waves. L-89316

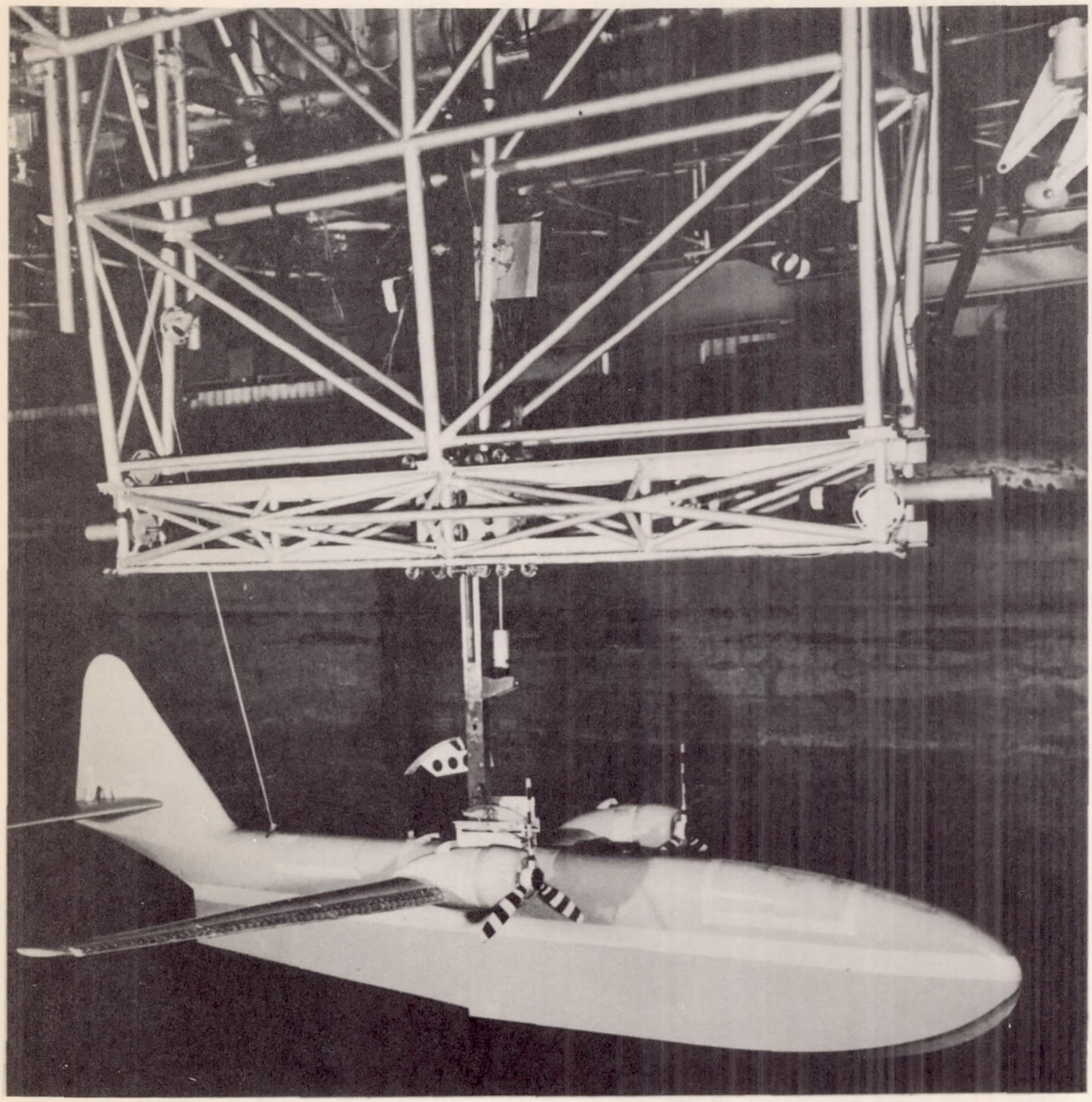

Figure 4.- View of model and apparatus. L-89317

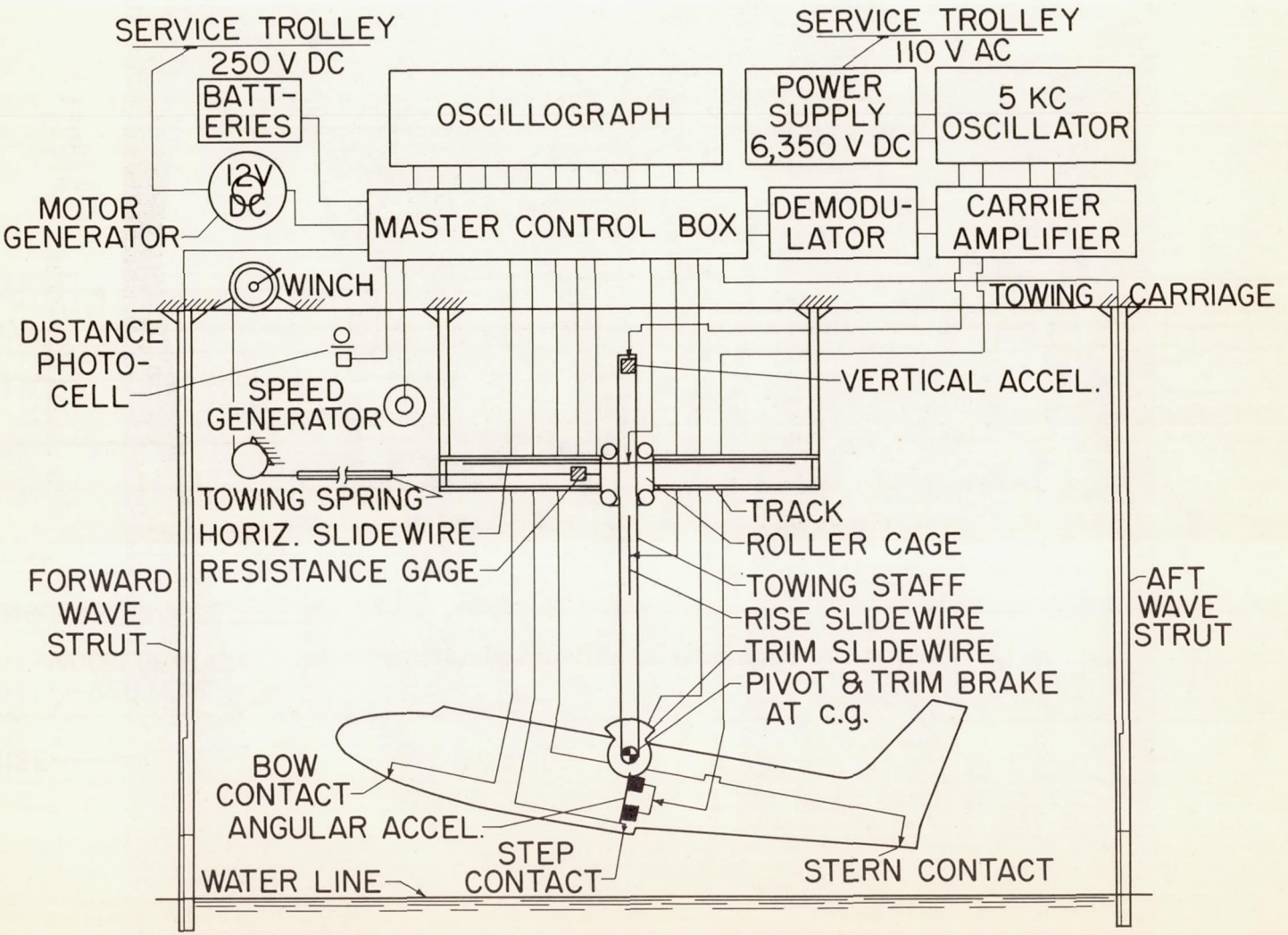

Figure 5.- Schematic diagram of apparatus and instrumentation.

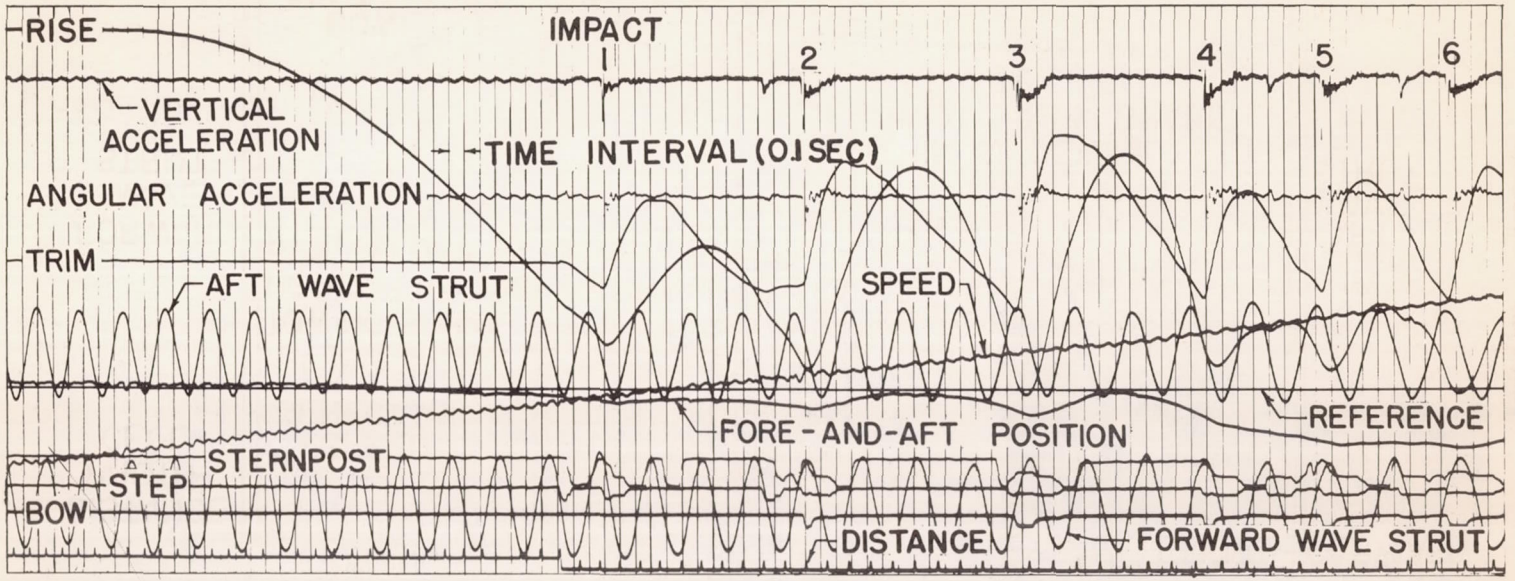

Figure 6.- Typical oscillograph record of landing.

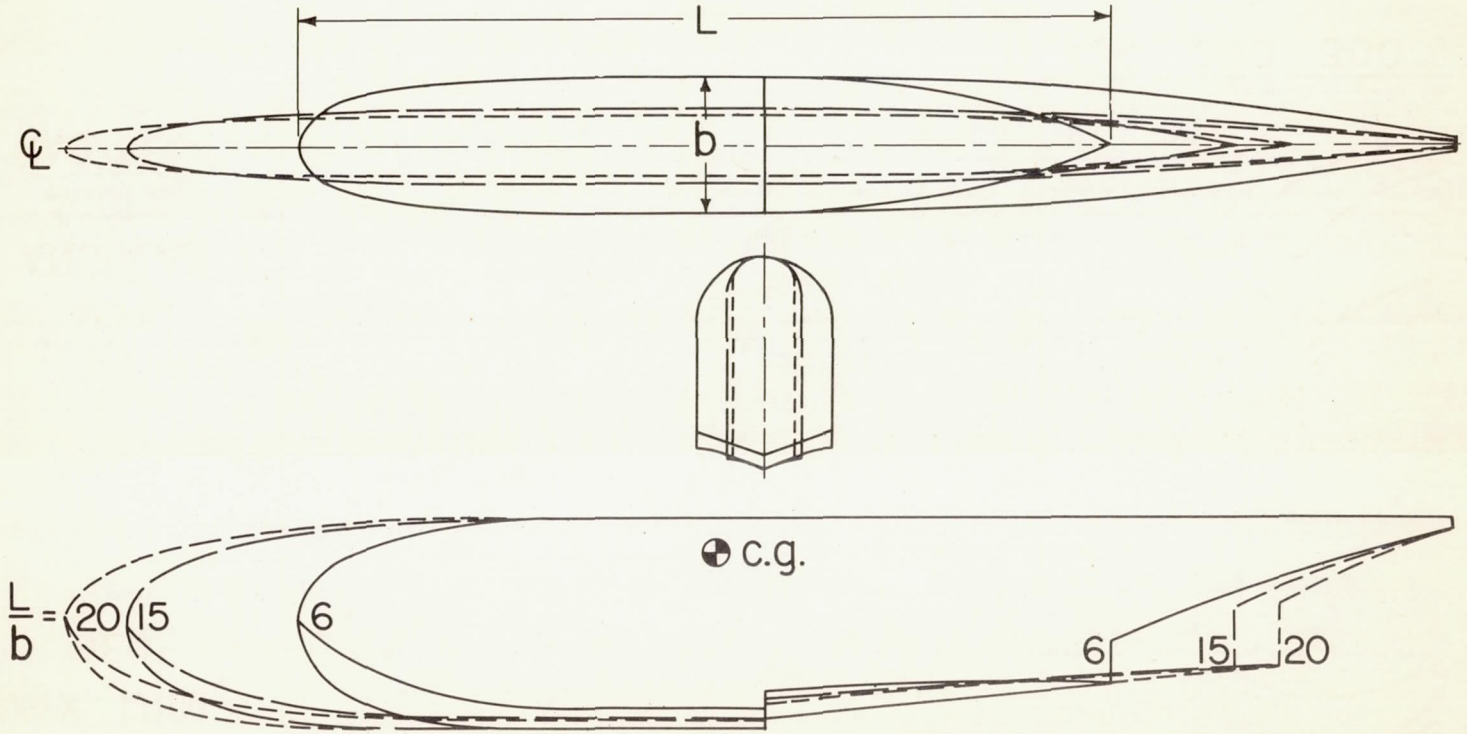

Figure 7.- Series of hulls of various length-beam ratios for the same flying boat.

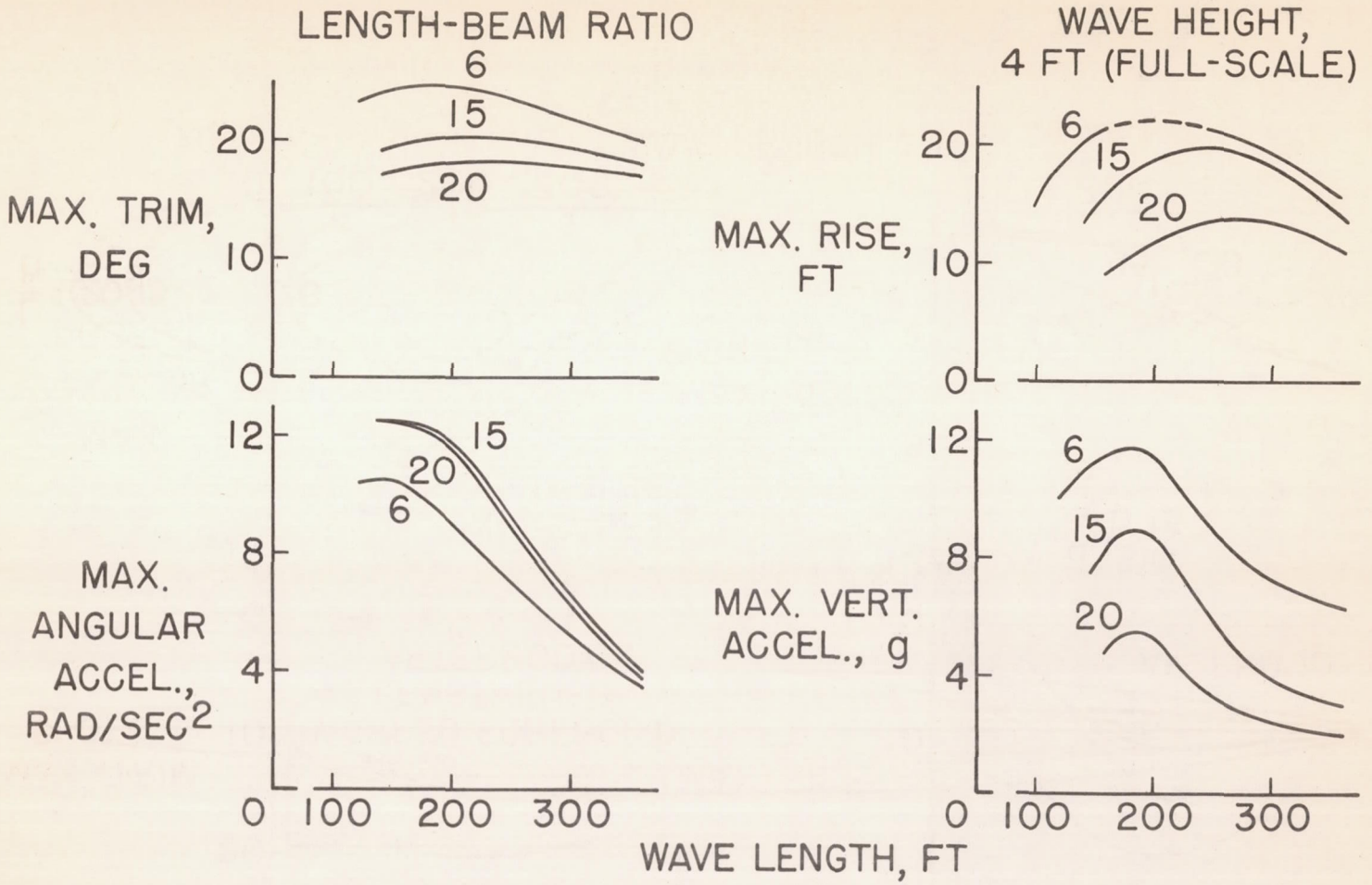

Figure 8.- Maximum motions and accelerations for three length-beam ratios. Data from references 7 and 8.

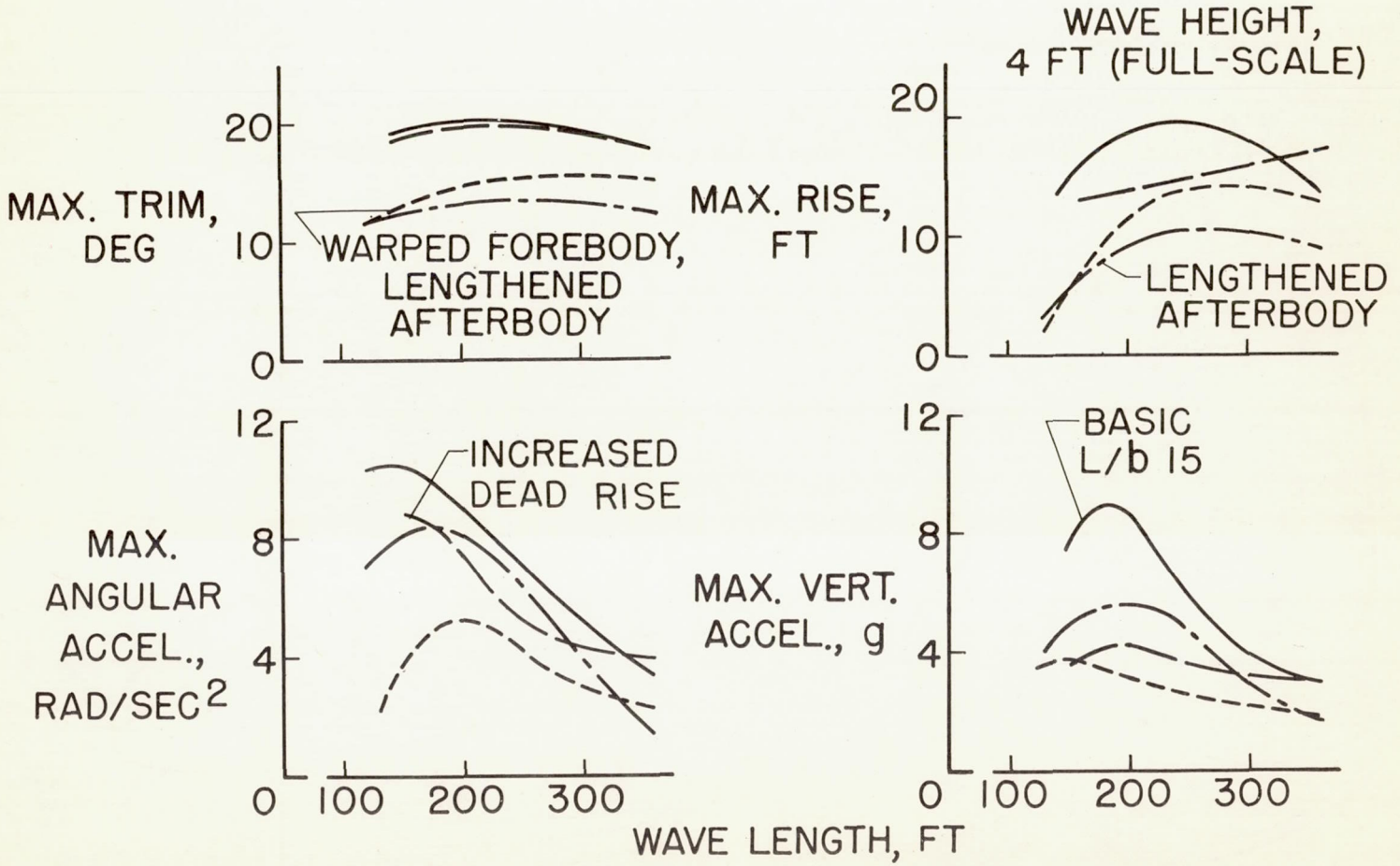

Figure 9.- Maximum motions and accelerations for modifications of the model with length-beam ratio of 15. Data from references 10, 11, and 12.

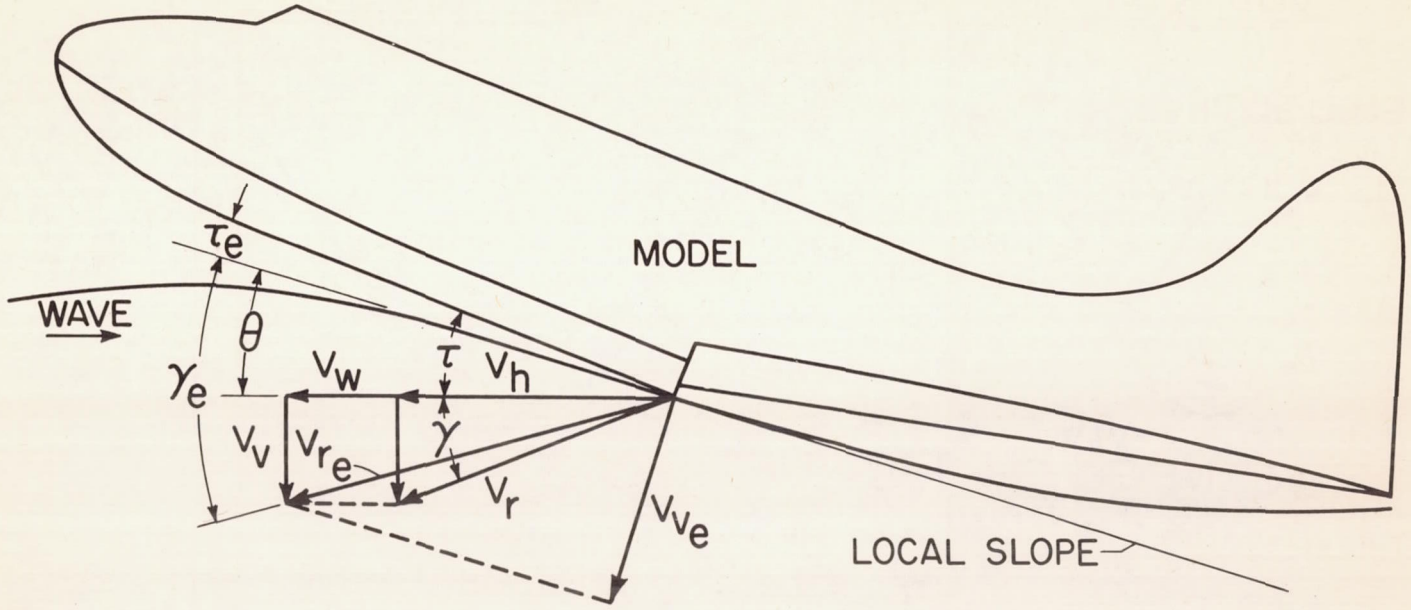

Figure 10.- Relation of geometric and effective contact parameters.

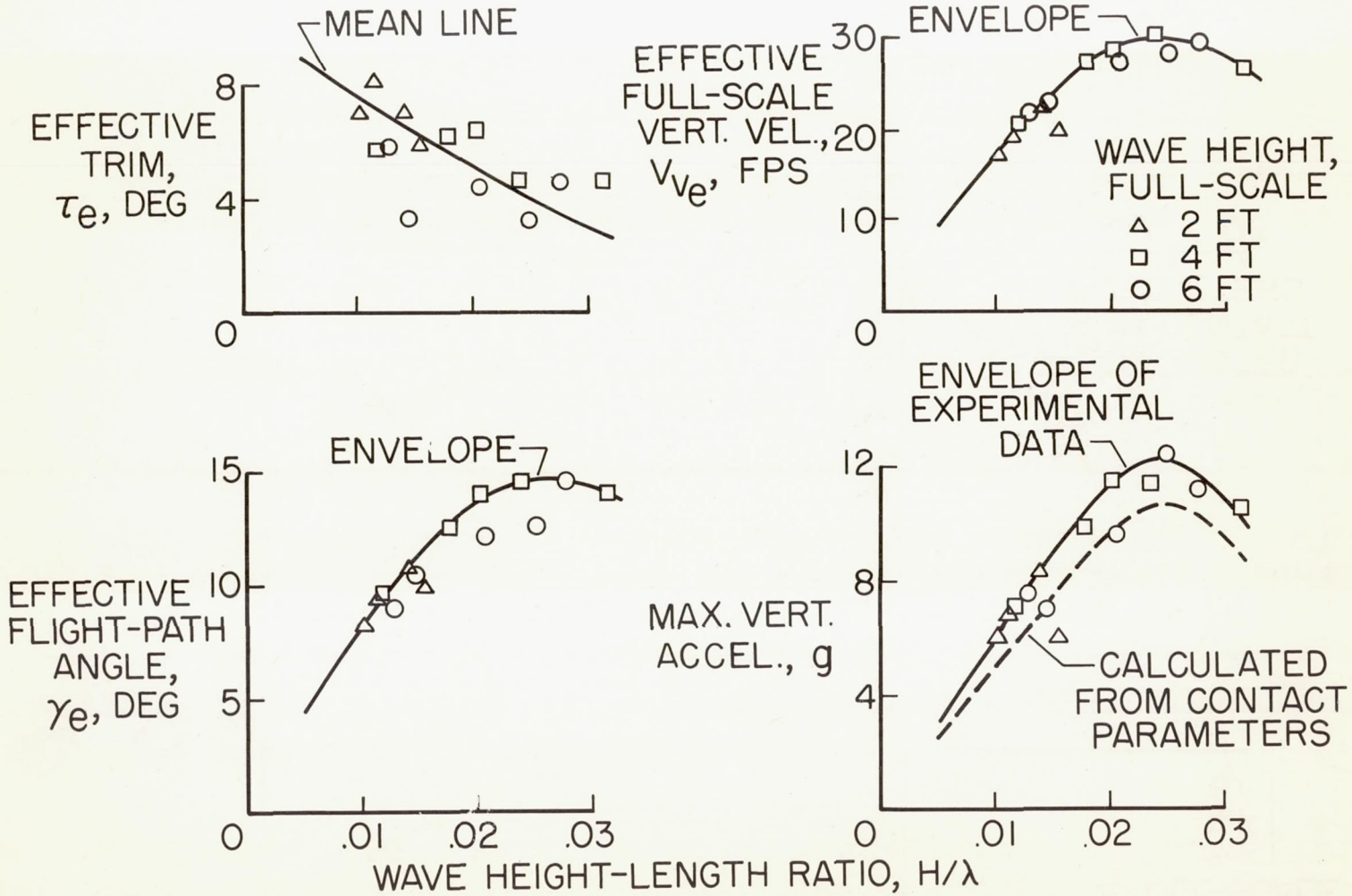

(a) Model with length-beam ratio of 6. Data from references 8 and 14.

Figure 11.- Effective contact parameters and maximum vertical accelerations.

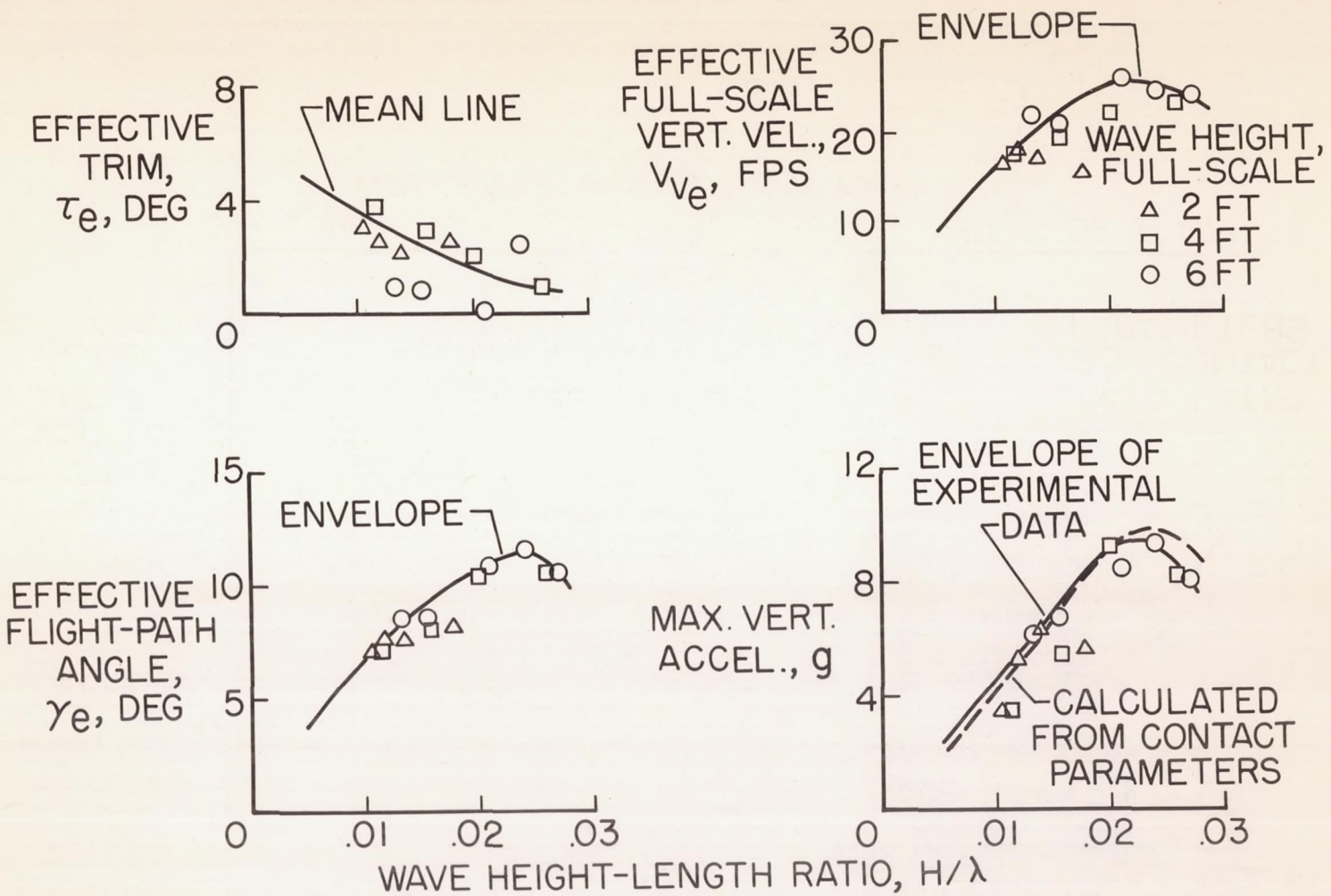

(b) Model with length-beam ratio of 15. Data from reference 8.

Figure 11.- Concluded.

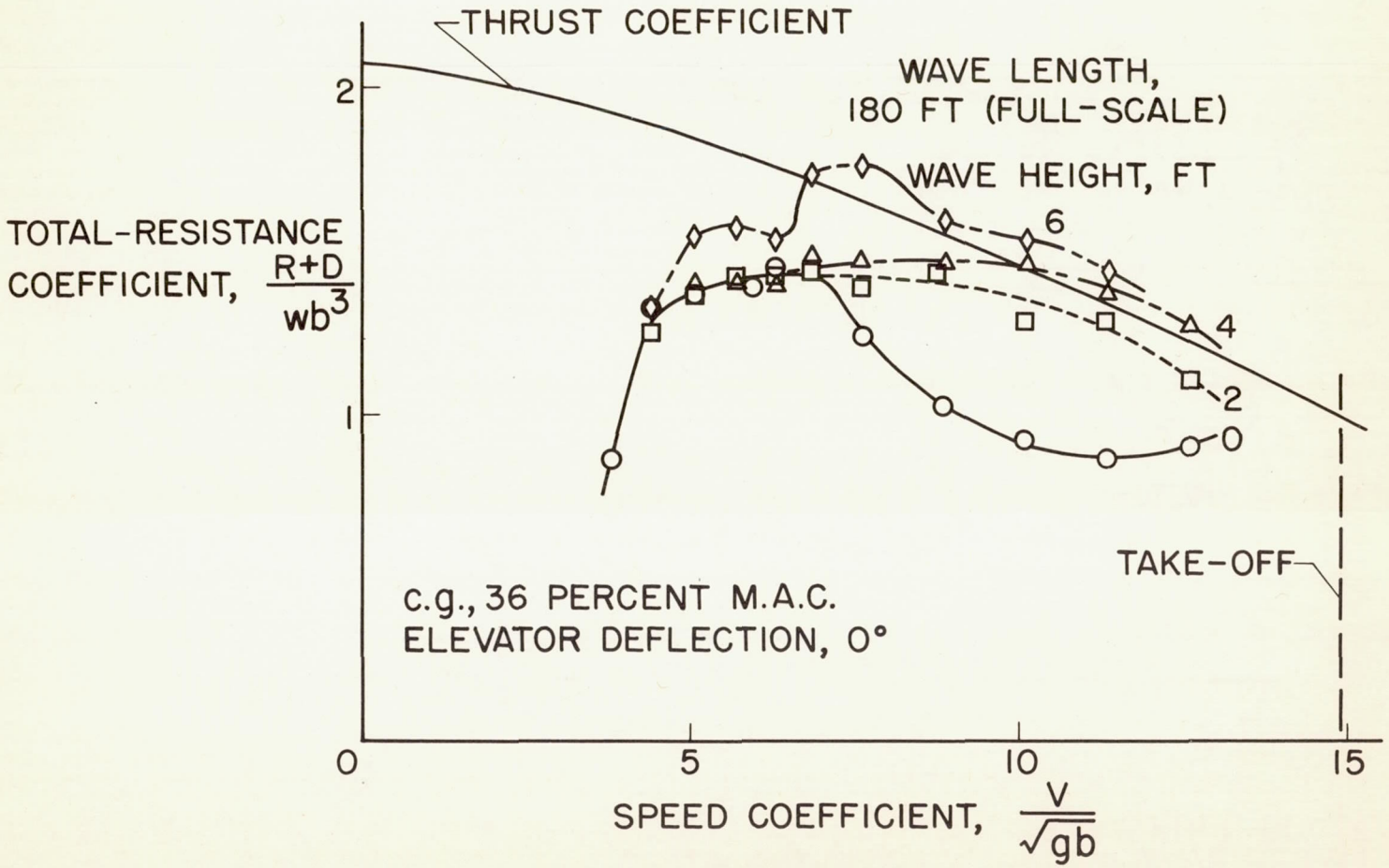

Figure 12.- Total resistance during take-off of model with length-beam ratio of 15.